

Influence of a chiral chemical potential on Weyl hybrid junctions

Daniel Breunig,¹ Song-Bo Zhang,^{1,*} Martin Stehno,² and Björn Trauzettel^{1,3}

¹*Theoretische Physik IV, Institut für Theoretische Physik und Astrophysik,
Universität Würzburg, D-97074 Würzburg, Germany*

²*Experimentelle Physik III, Physikalisches Institut,
Universität Würzburg, D-97074 Würzburg, Germany*

³*Würzburg-Dresden Cluster of Excellence ct.qmat, Germany*

(Dated: May 7, 2019)

We study the transport properties and superconducting proximity effect in NSN junctions formed by a time-reversal symmetry broken Weyl semimetal (WSM) in proximity to an s -wave superconductor. We find that the differential conductances and induced pairing amplitudes strongly depend on the angle between the junction direction in real space and the axis separating the Weyl nodes in momentum space. We identify the influence of a chiral chemical potential, i.e., the electron population imbalance between Weyl nodes of opposite chirality, on the transport characteristics of the junction. Remarkably, we observe a net spin polarization of Cooper pairs that are generated via Andreev reflection in the two WSM regions. The spin polarization is opposite in the two WSM regions and highly sensitive to the chirality imbalance and excitation energy.

I. INTRODUCTION

Weyl semimetals (WSMs), which are three-dimensional topological phases of matter with strong spin-orbit coupling, have been subject of intense research activities during the last years^{1–5}. They are featured by pairs of linear band crossings, called Weyl nodes, in momentum space. Since the Weyl nodes are topologically protected and closely associated with the chiral anomaly, WSMs impose a plethora of characteristic phenomena, such as surface Fermi arcs⁶, nonlocal transport⁷, and anomalous magnetoconductance^{8–13}. Moreover, there have been a growing number of realistic materials proposed theoretically^{14–25} and confirmed experimentally^{26–31} as WSMs. The proximity of materials with strong spin-orbit coupling to an s -wave superconductor can produce spin-triplet pairing which may give rise to topological superconductivity³². This implies intriguing physics, such as the emergence of odd-frequency superconductivity^{33–35} and Majorana bound states³². Among spin-triplet pairing, equal-spin pairing is of particular interest for superconducting spintronics³⁶ because it offers the potential to transfer and manipulate spin-polarized Cooper pairs. Recently, it has been put forward to generate equal-spin pairing in surface states of topological insulators without introducing magnetic order³⁷.

WSMs possess desirably strong spin-orbit coupling^{5,6}. It is therefore of fundamental interest and application potential for spintronics to explore the possibility of equal-spin pairing and related transport signatures in WSMs. There have been a few works studying the transport and pairing properties of superconducting heterostructures based on WSMs^{38–47}. However, the induced pairing in the WSM region is still poorly understood. Furthermore, previous studies focused only on the case where the electron populations at any Weyl nodes are the same. In principle, Weyl nodes of opposite chirality do not need to have the same electron population. In fact, an elec-

tron population imbalance between Weyl nodes of different chirality, called chiral chemical potential (CCP), can be achieved, e.g., by the chiral anomaly with applying parallel electric and magnetic fields^{8,48,49}, by a strain deformation^{50,51} or in a superlattice system with breaking both time-reversal and inversion symmetries⁵². This raises an important question of how the CCP influences the transport properties and superconducting proximity effect in Weyl heterostructures.

In this article, we investigate the transport and induced local pairing amplitudes in Weyl semimetal-superconductor-semimetal (NSN) junctions by using the scattering approach^{53–55}. In particular, we consider a WSM which breaks time-reversal symmetry and focus on the influence of a CCP. Due to the anisotropy of the band structure of the WSM, the differential conductances across the junction and the superconducting proximity effect strongly depend on the angle between the junction direction and the axis separating the Weyl nodes. The CCP shifts the excitation energy spectrum of the system and consequently changes the local and nonlocal differential conductances as a function of the bias voltage. The interplay of strong spin-orbit coupling and s -wave superconductivity in the system leads to the emergence of equal-spin pairing even deep inside the WSM regions. Interestingly, we find that for appropriate angles, the CCP gives rise to a large net spin polarization of Cooper pairs in the WSM regions. The spin polarization is opposite in the two WSM regions. It depends on the excitation energy, strength of the CCP and junction direction. This CCP-induced spin polarization of Cooper pairs with a dipole feature may find promising applications in superconducting spintronics.

The remainder of the paper is structured as follows. In Sec. II, we introduce the setup and model Hamiltonian. Then, we describe in Sec. III the scattering states for calculating the differential conductances and induced pairing amplitudes in the WSM regions. Sec. IV is dedicated to the results regarding the differential conductances, and

Sec. V to the results regarding pairing amplitudes and spin polarization of Cooper pairs in the WSM regions. Finally, we conclude and discuss the experimental relevance in Sec. VI.

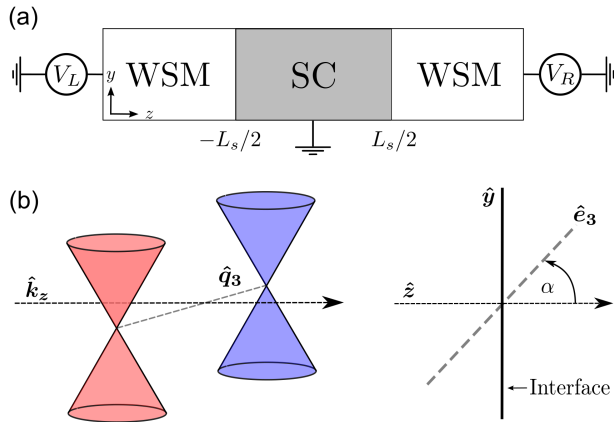


Fig. 1. (a) An NSN junction formed by a Weyl superconductor sandwiched by two WSM regions (or leads) along \hat{z} direction. The superconductor is grounded while the two WSM regions are connected to the voltage sources V_L and V_R , respectively. (b) The junction direction \hat{z} deviates from the axis \hat{e}_3 separating the Weyl nodes by an angle α . The blue and red colored cones, separated in \hat{q}_3 direction, denote the Weyl fermions of positive and negative chirality, respectively.

II. SETUP AND MODEL

We consider an NSN junction formed by a Weyl superconductor sandwiched between two leads of WSMs, as illustrated in Fig. 1(a). The left and right WSM regions extend semi-infinitely along \hat{z} direction and are connected to the voltage sources V_L and V_R , respectively. The superconductor is grounded. The interfaces between WSMs and superconductor, located at $z_L \equiv -L_s/2$ and $z_R \equiv L_s/2$, are assumed to extend along the xy -plane. We consider the simplest WSM with a single pair of Weyl nodes. The minimal model at low energies is given by

$$H_0 = \sum_{\tau=\pm} \sum_{\mathbf{q}} \Psi_{\tau\mathbf{q}}^\dagger H_{\tau}(\mathbf{q}) \Psi_{\tau\mathbf{q}}, \quad (1)$$

$$H_{\pm}(\mathbf{q}) = v_F [q_1 s_1 + q_2 s_2 \mp (q_3 \mp K_0) s_3] - \mu s_0, \quad (2)$$

where v_F is the Fermi velocity which we take as $v_F \equiv 1$; μ is the chemical potential; $\tau = \pm$ denotes the Weyl nodes of positive and negative chirality, respectively; s_0 and $s_{1,2,3}$ are unit and Pauli matrices acting on the spin space, respectively. $\Psi_{\tau\mathbf{q}}^\dagger = (c_{\uparrow,\tau,\mathbf{q}}^\dagger, c_{\downarrow,\tau,\mathbf{q}}^\dagger)$ is the spinor basis for Weyl nodes with $c_{s,\tau,\mathbf{q}}^\dagger$ the creation operator for an electron with spin s and momentum \mathbf{q} at node τ . $\sum_{\mathbf{q}}$ means that \mathbf{q} is restricted to the momenta in the vicinity of the nodes. The two Weyl nodes are related by inversion symmetry, as indicated by $s_z H_+(\mathbf{q}) s_z = H_-(-\mathbf{q})$. Without

loss of generality, we assume that the pair of Weyl nodes are separated in the \hat{e}_3 crystalline axis, $\mathbf{K}_0 = \pm K_0 \hat{q}_3$. The model (2) also features a rotational symmetry with respect to the \hat{e}_3 axis. In general, the crystal coordinates are different from the junction coordinates. To describe this, we introduce the angle α between the junction direction \hat{z} and the \hat{e}_3 axis. For the junction problems, it is convenient to work with the junction coordinates $\mathbf{r} = (x, y, z)$ (correspondingly, $\mathbf{k} = (k_x, k_y, k_z)$ in momentum space). The two coordinate systems are related by a rotation matrix with respect to \hat{y} direction, which is given by

$$\hat{R} = \begin{pmatrix} \cos \alpha & 0 & -\sin \alpha \\ 0 & 1 & 0 \\ \sin \alpha & 0 & \cos \alpha \end{pmatrix}. \quad (3)$$

Explicitly, we use the rotation $(q_x, q_y, q_z)^T = \hat{R}(k_x, k_y, k_z)^T$ and $(s_1, s_2, s_3)^T = \hat{R}(\sigma_x, \sigma_y, \sigma_z)^T$ with T meaning the transpose.

We consider Bardeen-Cooper-Schrieffer (BCS)-like pairing in the superconductor, which may be induced by the proximity to a conventional superconductor^{40,56}. At low energies, the pairing term reads

$$H_P = \sum_{\mathbf{q}}' (\Delta c_{\uparrow,+,\mathbf{q}}^\dagger c_{\downarrow,-,-\mathbf{q}}^\dagger + h.c.), \quad (4)$$

where Δ is the pairing potential. The pairing potential couples excitations at one Weyl node to those at the other node. Combining the model (2) with the pairing term in Eq. (4), the Bogoliubov-de Gennes (BdG) Hamiltonian for the system can be written as two decoupled blocks \mathcal{H}^\pm in the basis $(c_{\uparrow,+,\mathbf{k}}^\dagger, c_{\downarrow,+,\mathbf{k}}^\dagger, c_{\downarrow,-,-\mathbf{k}}, -c_{\uparrow,-,-\mathbf{k}})$ and $(c_{\uparrow,-,-\mathbf{k}}^\dagger, c_{\downarrow,-,-\mathbf{k}}^\dagger, c_{\downarrow,+,-\mathbf{k}}, -c_{\uparrow,+,-\mathbf{k}})$ in the junction coordinates, respectively. The two blocks are related by particle-hole symmetry. For a uniform pairing potential, the system realizes a Weyl superconductor^{56,57} with four Weyl nodes in the BdG spectrum. We next perform the unitary transformations

$$\mathcal{H}^\pm \rightarrow \hat{U}_\alpha^\pm \mathcal{H}^\pm (\hat{U}_\alpha^\pm)^{-1} \quad (5)$$

with

$$\hat{U}_\alpha^\pm = \frac{1}{2} [(\tau_0 \pm \tau_z) \sigma_x e^{i\alpha \sigma_y} + (\tau_0 \mp \tau_z) \sigma_0] e^{\pm i K_0 \cdot r}, \quad (6)$$

where τ_0 and $\tau_{x,y,z}$ are unit and Pauli matrices in particle-hole space, respectively. Then, the K_0 -dependence is moved into the basis wavefunctions and the α -dependence into the order parameter. The resulting BdG Hamiltonians \mathcal{H}^\pm become

$$\mathcal{H}^\pm = \begin{pmatrix} k_z - \mu & k_x \pm i k_y & -\Delta \sin \alpha & \Delta \cos \alpha \\ k_x \mp i k_y & -k_z - \mu & \Delta \cos \alpha & \Delta \sin \alpha \\ -\Delta \sin \alpha & \Delta \cos \alpha & \mu - k_z & -k_x \pm i k_y \\ \Delta \cos \alpha & \Delta \sin \alpha & -k_x \mp i k_y & \mu + k_z \end{pmatrix}. \quad (7)$$

In the NSN junction, the chemical and pairing potentials are spatially dependent. For simplicity, we assume a step-like model for these potentials

$$\mu(z) = \mu_N \Theta(|z| - L_s/2) + \mu_S \Theta(L_s/2 - |z|), \quad (8)$$

$$\Delta(z) = \Delta_0 \Theta(L_s/2 - |z|), \quad (9)$$

which is justified when the chemical potential μ_S in the superconductor is much larger than that in the WSM regions^{58,59}. Also to satisfy the mean-field approximation for Δ_0 , a heavily doped superconductor is assumed. Thus, in this work, we focus on the case with $|\mu_S| \gg |\mu_N|, \Delta_0$. A CCP between the two Weyl nodes, which can be induced by applying parallel electric and magnetic fields via the chiral anomaly^{8,48,49} or by a strain deformation^{50,51}, can be taken into account by introducing a term $\mp \chi s_0$ in H_{\pm} in Eq. (2), respectively, where χ measures the strength of the chirality imbalance. This CCP breaks the inversion symmetry of the model and requires an additional term

$$\mathcal{H}_{\chi}^{\pm} = \mp \chi \tau_0 \sigma_0 \quad (10)$$

in the BdG Hamiltonian \mathcal{H}^{\pm} in Eq. (7). To illustrate the main effect of the CCP and for simplicity, we consider a constant χ everywhere in the junction. Then, the CCP leads to opposite energy shifts in the excitation spectra of the two blocks \mathcal{H}^{\pm} . This essential mechanism results in interesting phenomena with respect to transport and induced pairing amplitudes as we will discuss below.

III. SCATTERING STATES

To study the transport properties and superconducting proximity effect in the Weyl NSN junction, we apply the scattering approach^{53–55}. Due to the translational invariance parallel to the interfaces, the scattering modes with different transverse wave vectors $\mathbf{k}_{\parallel} = (k_x, k_y)$ can be treated separately. In the following, we take the \mathcal{H}^+ block to illustrate the calculations. The results for the other block \mathcal{H}^- can be obtained from those for \mathcal{H}^+ by exploiting the particle-hole symmetry between them. The

four scattering states for \mathcal{H}^+ are built up as

$$\phi_{1/2}(z) = \begin{cases} \psi_{e/h}^{\rightarrow}(z) + a_{1/2} \psi_{h/e}^{\leftarrow}(z) \\ + b_{1/2} \psi_{e/h}^{\leftarrow}(z), & z < z_L, \\ \sum_{i=1}^4 s_{1/2,i} \psi_i^S(z), & |z| < z_R, \\ c_{1/2} \psi_{e/h}^{\rightarrow}(z) + d_{1/2} \psi_{h/e}^{\leftarrow}(z), & z > z_R, \end{cases} \quad (11a)$$

$$\phi_{3/4}(z) = \begin{cases} c_{3/4} \psi_{e/h}^{\leftarrow}(z) + d_{3/4} \psi_{h/e}^{\leftarrow}(z), & z < z_L, \\ \sum_{i=1}^4 s_{3/4,i} \psi_i^S(z), & |z| < z_R, \\ \psi_{e/h}^{\leftarrow}(z) + a_{3/4} \psi_{h/e}^{\rightarrow}(z) \\ + b_{3/4} \psi_{e/h}^{\rightarrow}(z), & z > z_R, \end{cases} \quad (11b)$$

where $\phi_{1/2}(z)$ describes an electron/hole excited in the left lead moving towards the interface, while $\phi_{3/4}(z)$ describes the corresponding processes in the right lead. We omit the factor $e^{ik_x x + ik_y y}$ for convenience. a_j, b_j, c_j and d_j with $j \in \{1, 2, 3, 4\}$ are amplitudes of Andreev reflection, normal reflection, electron co-tunneling and crossed Andreev reflection, respectively, while $s_{j,i}$ with $i \in \{1, 2, 3, 4\}$ are the scattering amplitudes in the superconducting region. These amplitudes are determined by matching the wavefunctions at the interfaces $z = z_{L/R}$,

$$\phi_j(z_{L/R} - 0^+) = \phi_j(z_{L/R} + 0^+). \quad (12)$$

The basis wavefunctions in the WSMs are given by

$$\psi_{\vec{e}}(z) = (J_e, k_{\parallel} e^{-i\theta_k}, 0, 0)^T e^{ik_e z}, \quad (13a)$$

$$\psi_{\vec{e}}(z) = (k_{\parallel} e^{i\theta_k}, J_e, 0, 0)^T e^{-ik_e z}, \quad (13b)$$

$$\psi_{\vec{h}}(z) = (0, 0, k_{\parallel} e^{-i\theta_k}, -J_h)^T e^{ik_h z}, \quad (13c)$$

$$\psi_{\vec{h}}(z) = (0, 0, J_h, -k_{\parallel} e^{i\theta_k})^T e^{-ik_h z}, \quad (13d)$$

where $k_{e/h} = \zeta_{e/h} \sqrt{(\varepsilon + \chi \pm \mu_N)^2 - k_{\parallel}^2}$, $J_{e/h} = k_{e/h} + \varepsilon + \chi \pm \mu_N$, $k_{\parallel} = |\mathbf{k}_{\parallel}|$ and $\theta_k = \arg(k_y/k_x)$. The alphabetical subscript e/h distinguishes electrons from holes, the arrows point in the direction of propagation (with respect to \hat{z} direction) and $\zeta_{e/h} = \text{sign}(\varepsilon + \chi \pm \mu_N + k_{\parallel})$ indicates whether the particle stems from the valence or the conduction band.

The basis wavefunctions in the superconductor, in general, can also be found analytically, but are too extensive to be displayed here. However, under the assumption of a large chemical potential mismatch, $|\mu_S| \gg |\mu_N|$, all excitations show quasi-perpendicular ($k_{\parallel} \approx 0$) transmission into the superconductor. In this regime, we can approx-

imate the basis wavefunctions as

$$\psi_1^S(z) = (K_e, 0, -\Delta_0 \sin \alpha, 0)^T e^{ik_q z} e^{i\mu_S z}, \quad (14a)$$

$$\psi_2^S(z) = (0, K_e, 0, \Delta_0 \sin \alpha)^T e^{-ik_q z} e^{-i\mu_S z}, \quad (14b)$$

$$\psi_3^S(z) = (0, \Delta_0 \sin \alpha, 0, K_e)^T e^{ik_q z} e^{-i\mu_S z}, \quad (14c)$$

$$\psi_4^S(z) = (\Delta_0 \sin \alpha, 0, K_e, 0)^T e^{-ik_q z} e^{i\mu_S z}, \quad (14d)$$

where $K_e = \varepsilon + \chi + k_q$ and $k_q = \sqrt{(\varepsilon + \chi)^2 - \Delta_0^2 \sin^2 \alpha}$. Evidently, the effective superconducting gap depends on the angle α as $\tilde{\Delta}_0 \equiv \Delta_0 |\sin \alpha|$. Hence, it vanishes for integer multiples and is maximal for half integer multiples of π . This angle dependence reflects the

anisotropy of the band structure and may be regarded as a characteristic feature of BCS-like superconductivity in time-reversal symmetry broken Weyl hybrid structures^{38,44,47}.

IV. DIFFERENTIAL CONDUCTANCE

With the scattering amplitudes a_j, b_j, c_j and d_j , we are ready to calculate the differential conductances across the junction. The local and non-local (differential) conductances, defined as $G_{LL} \equiv dI_L/dV_L|_{V_R=0}$ and $G_{LR} \equiv dI_R/dV_L|_{V_R=0}$, respectively, at zero temperature can be written in terms of scattering probabilities^{60,61}

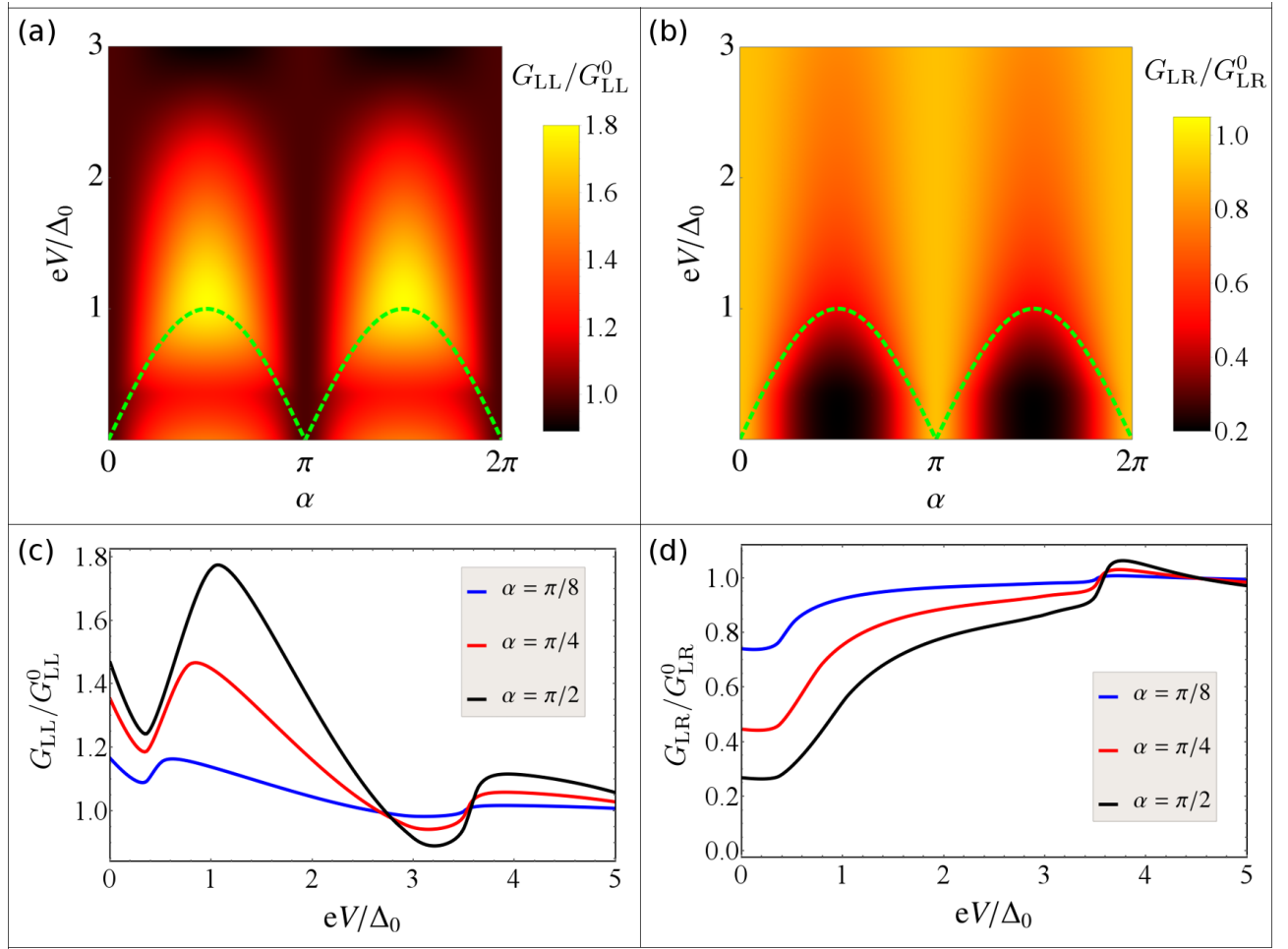


Fig. 2. Contour plots of the (a) local and (b) non-local conductances $\bar{G}_{L\Lambda}$ with $\Lambda \in \{L, R\}$ as functions of the angle α and bias voltage eV . The green dashed curves indicate the effective superconducting gap $\tilde{\Delta}_0(\alpha)$. (c) Local and (d) non-local conductances $\bar{G}_{L\Lambda}$ as functions of eV for different choices of α . For different $\alpha (\notin \{0, \pi\})$, the curves of $\bar{G}_{L\Lambda}(eV)$ are qualitatively the same. $\mu_S = 10^6 \Delta_0$, $\mu_N = 10^3 \Delta_0$, $\chi = 0$ and $L_s = \xi$ for all plots.

$$G_{LL} = \frac{2e^2}{h} \sum_{\mathbf{k}_{\parallel}} (1 + R_{eh} - R_{ee}), \quad (15a)$$

$$G_{LR} = \frac{2e^2}{h} \sum_{\mathbf{k}_{\parallel}} (T_{ee} - T_{eh}), \quad (15b)$$

where the sum runs over all relevant \mathbf{k}_{\parallel} that allow incident channels⁶². The probabilities of the four relevant

processes for an incident electron from the left are given by

$$R_{ee} = |b_1|^2, \quad (16a)$$

$$R_{eh} = \frac{J_h \operatorname{Re}(k_h)}{J_e k_e} |a_1|^2, \quad (16b)$$

$$T_{ee} = |c_1|^2, \quad (16c)$$

$$T_{eh} = \frac{J_h \operatorname{Re}(k_h)}{J_e k_e} |d_1|^2. \quad (16d)$$

Let us assume a bias voltage $V_L = V$ is applied to the left lead and keep the right lead unbiased $V_R = 0$. The bias voltage V enters the formulas (15a) and (15b) as the excitation energy $\varepsilon \rightarrow eV$ via the scattering probabilities. For definiteness and experimental feasibility, we consider a large chemical potential in the WSMs compared to the pairing potential and CCP, i.e., $|\mu_N| \gg \Delta_0, \chi$. To manifest the non-local transport, we choose a junction length comparable to the coherence length of the superconductor, $L_s = \xi \equiv v_F/\Delta_0$. We note that the main results discussed below do not change qualitatively for other choices of μ_N or L_s . In the following, we normalize the local and non-local conductances $\bar{G}_{\Lambda} \equiv G_{\Lambda}/G_{\Lambda}^0$, $\Lambda \in \{L,R\}$ with respect to their normal counterparts G_{Λ}^0 at $\Delta_0 = 0$, respectively.

For comparison, we first discuss some universal features of \bar{G}_{Λ} in the absence of a CCP. The results of \bar{G}_{Λ} are shown Fig. 2 as functions of the angle α and bias voltage eV . First of all, both \bar{G}_{Λ} are π -periodic functions of α and obey a symmetry with respect to α , $\bar{G}_{\Lambda}(\alpha) = \bar{G}_{\Lambda}(\pi - \alpha)$. This angle dependence reflects the strength of the effective superconducting gap which scales as $\tilde{\Delta}_0 = \Delta_0 |\sin \alpha|$. For $\alpha = 0, \pi$, Andreev and cross-Andreev reflection processes are completely suppressed and the same characteristics as for a Weyl NN'N junction with $\Delta_0 = 0$ are observed. For $\alpha = \pi/2$ ($\tilde{\Delta}_0 \approx \Delta_0$), Andreev and crossed Andreev reflections occur with prominent probabilities in the sub-gap region ($eV < \tilde{\Delta}_0$), while the normal transport is quickly restored in the supra-gap region ($eV > \tilde{\Delta}_0$). Unlike the normalized conductance in Weyl NS junctions³⁸, the normalized local conductance is no longer a constant in the sub-gap region, as the incoming particles can tunnel from one WSM region into the other. Instead, the conductances \bar{G}_{Λ} vary substantially and show oscillatory behavior which stems from the interference effect in the junction. The local conductance G_{LL} is larger than G_{LL}^0 for $\alpha \neq 0, \pi$ inside the gap due to the contribution of Andreev reflection. However, the non-local conductance G_{LR} is reduced by crossed Andreev reflection, as indicated by Eqs. (15a) and (15b). At zero bias voltage, \bar{G}_{LL} exhibits a pronounced peak whereas \bar{G}_{LR} has a flat valley, as shown in Fig. 2(c) and (d). Outside the sub-gap region, G_{Λ} recover their normal values G_{Λ}^0 . The oscillatory behavior is reduced if we consider a longer junction or an angle α close to 0 or π . Finally, we note that in the absence of a CCP, both \bar{G}_{Λ} are even functions of eV . The contributions from \mathcal{H}^{\pm} are identical. Thus, the measured conductances are

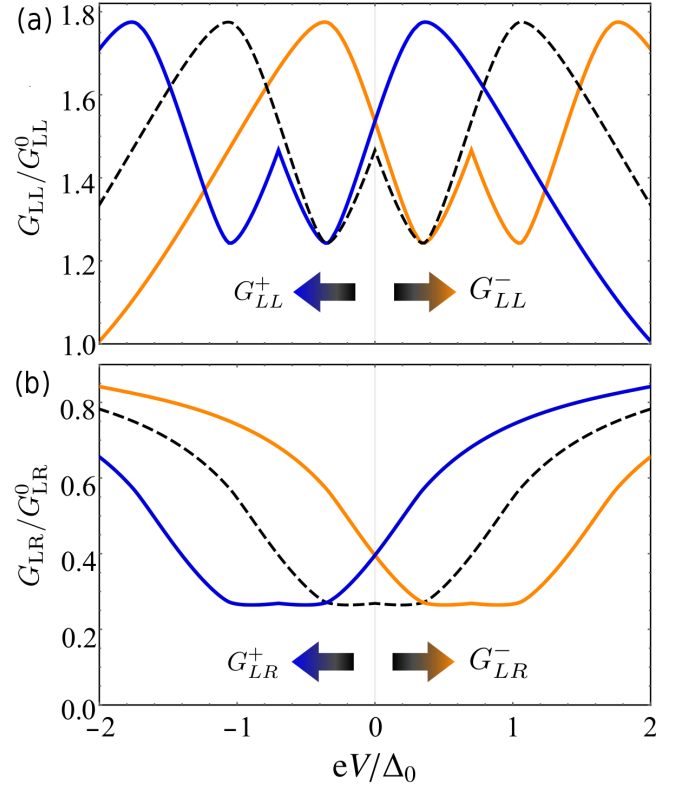


Fig. 3. (a) Local and (b) non-local conductances \bar{G}_{Λ}^{\pm} as functions of the bias voltage eV . The black dashed curves are for the absence of a CCP, $\chi = 0$. The blue and orange solid curves are \bar{G}_{Λ}^{\pm} with $\Lambda \in \{L,R\}$ in the presence of $\chi = 0.7\Delta_0$, respectively. The CCP shifts the curves of $\bar{G}_{\Lambda}^{\pm}(eV)$ in the eV axis oppositely. Here, $\alpha = \pi/2$ and other parameters are the same as those in Fig. 2.

just twice the conductances from \mathcal{H}^+ .

A finite CCP enters as opposite energy shifts in the excitation energy spectra of \mathcal{H}^{\pm} and hence results in opposite shifts with respect to the bias voltage, $eV \rightarrow eV \pm \chi$. Consequently, the conductances G_{Λ}^{\pm} from the two blocks \mathcal{H}^{\pm} become different and are no longer even functions of eV , see Fig. 3. However, the relations between them, $G_{\Lambda}^-(\chi, eV) = G_{\Lambda}^+(\chi, -eV)$, are preserved since the CCP does not break particle-hole symmetry. Therefore, the total conductances of the system,

$$G_{\Lambda}^{\Sigma}(\chi, eV) = G_{\Lambda}^+(\chi, eV) + G_{\Lambda}^-(\chi, eV), \quad (17)$$

are still even functions of eV . For large bias voltages $eV \gg \chi$, the normalized conductances $\bar{G}_{\Lambda}^{\Sigma} \equiv G_{\Lambda}^{\Sigma}/G_{\Lambda}^{\Sigma,0}$, recover their values in the absence of CCP, as shown in Fig. 4(a) and (b). However, substantial modifications emerge within the small bias voltage window $|eV| \lesssim \chi$. In the local conductance \bar{G}_{LL}^{Σ} , more peaks with reduced amplitudes appear, while in the nonlocal conductance \bar{G}_{LR}^{Σ} , the valley at zero bias voltage becomes wider and small oscillations become possible. At zero bias voltage, G_{Λ}^+ and G_{Λ}^- are always the same, as protected by particle-hole symmetry. Thus, the total zero-bias conductances is

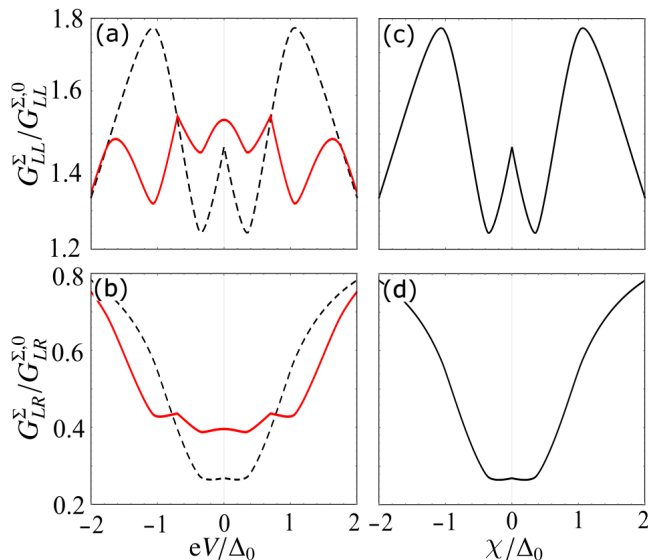


Fig. 4. Total (a) local and (b) non-local conductances \bar{G}_{LL}^{Σ} as functions of the bias voltage eV . The black dashed and red solid curves are for the absence and presence of a CCP $\chi = 0.7\Delta_0$, respectively. \bar{G}_{LL}^{Σ} are always even functions of eV . Total zero-bias (c) local and (d) non-local conductances \bar{G}_{LR}^{Σ} as functions of the CCP χ . Here, $\alpha = \pi/2$ and other parameters are the same as those in Fig. 2.

simply twice the value of G_{LA}^{\pm} . In Fig. 4(c) and (d), we plot the total zero-bias conductances $\bar{G}_{LA}^{\Sigma}(\chi, 0)$ as functions of the CCP χ . Due to the general relations between G_{LA}^{\pm} , $\bar{G}_{LA}^{\Sigma}(\chi, 0)$ take the exactly the same shapes as $\bar{G}_{LA}^{\Sigma}(0, eV)$. Both $\bar{G}_{LA}^{\Sigma}(\chi, 0)$ are also even functions of χ . A small χ retains almost the same nonlocal conductance $\bar{G}_{LR}^{\Sigma}(0, eV)$ but changes the local one $\bar{G}_{LL}^{\Sigma}(0, eV)$ quickly. With increasing χ further, both $\bar{G}_{LA}^{\Sigma}(0, eV)$ gradually relax to unity where the superconducting effect becomes negligible. From this point of view, the CCP plays a similar role as the bias voltage and may be used to control the transport in the Weyl junction. Note that one could introduce the CCP by applying a uniform parallel electromagnetic field^{8,48} or a strain deformation^{50,51} to the junction, and tune the strength of the CCP via the field strength. Moreover, the conductance modification by the applied fields in the small bias voltage regime can also serve to detect the CCP.

V. INDUCED PAIRING AMPLITUDES

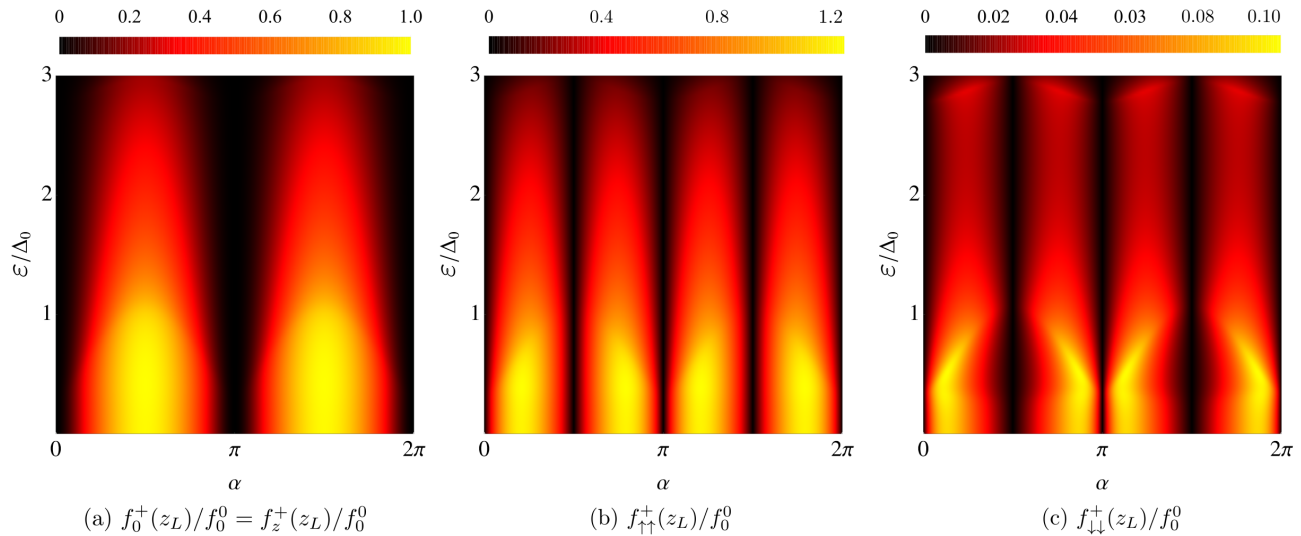


Fig. 5. Local pairing amplitudes as functions of the angle α and energy ε . (a) opposite-spin amplitudes $f_0^+(z_L)/f_0^0 = f_z^+(z_L)/f_0^0$, equal-spin amplitudes (b) $f_{1\uparrow}^+(z_L)/f_0^0$ and (c) $f_{1\downarrow}^+(z_L)/f_0^0$ at the left interface $z_L = -L_s/2$. All amplitudes are normalized by f_0^0 , the zero-energy value of $f_0^+(z_L)$. We choose $\mu_S = 10^6\Delta_0$, $\mu_N = 10^3\Delta_0$, $\chi = 0$ and $L_s = \xi$ for all figures.

We now proceed to discuss the induced pairing amplitudes in the WSM regions. The pairing amplitudes are contained in the anomalous Green's function (the electron-hole part of the Green's function in Nambu space). The retarded Green's function can be con-

structed by combining the scattering states^{37,53,55}

$$\mathcal{G}^R(z, z') = \begin{cases} \alpha_1\phi_3(z)\tilde{\phi}_1^T(z') + \alpha_2\phi_3(z)\tilde{\phi}_2^T(z') \\ + \alpha_3\phi_3(z)\tilde{\phi}_1^T(z') + \alpha_4\phi_3(z)\tilde{\phi}_2^T(z'), & z < z' \\ \beta_1\phi_1(z)\tilde{\phi}_3^T(z') + \beta_2\phi_1(z)\tilde{\phi}_4^T(z') \\ + \beta_3\phi_2(z)\tilde{\phi}_3^T(z') + \beta_4\phi_2(z)\tilde{\phi}_4^T(z'), & z > z' \end{cases} \quad (18)$$

where $\phi_l(z)$ with $l \in \{1, 2, 3, 4\}$ are given by Eqs. (11), while $\tilde{\phi}_l(z)$ are the scattering states of the transposed Hamiltonian $(\mathcal{H}^+)^T$, which can be obtained analytically in a similar way. Note that \mathcal{G}^R are also functions of other variables such as ε , α , χ and \mathbf{k}_\parallel . The spatial dependence is shown explicitly in Eq. (18) because it is important to determine the coefficients α_l and β_l . Requiring the discontinuity of $\mathcal{G}^R(z, z')$ at any position $z = z'$ across the junction,

$$\mathcal{G}^R(z, z - 0^+) - \mathcal{G}^R(z, z + 0^+) = -i\tau_z \sigma_z, \quad (19)$$

α_l and β_l are analytically derived as

$$\alpha_1 = \beta_1 = -\frac{i}{J_e k_e} \frac{c_4}{c_3 c_4 - d_3 d_4}, \quad (20a)$$

$$\alpha_2 = \beta_2 = \frac{i}{J_h k_h} \frac{d_4}{c_3 c_4 - d_3 d_4}, \quad (20b)$$

$$\alpha_3 = \beta_3 = \frac{i}{J_e k_e} \frac{d_3}{c_3 c_4 - d_3 d_4}, \quad (20c)$$

$$\alpha_4 = \beta_4 = -\frac{i}{J_h k_h} \frac{c_3}{c_3 c_4 - d_3 d_4}. \quad (20d)$$

Transforming back to the original spin space, the retarded anomalous Green's function can be written in a 2×2 matrix of the general form

$$F(z, z') = \tilde{f}_0^+(z, z') s_0 + \tilde{f}_{\uparrow\uparrow}^+(z, z') (s_x + i s_y) + \tilde{f}_{\downarrow\downarrow}^+(z, z') (s_x - i s_y) + \tilde{f}_z^+(z, z') s_z. \quad (21)$$

The functions \tilde{f}_s^+ with $s \in \{0, z, \uparrow\uparrow, \downarrow\downarrow\}$ correspond to the pairing amplitudes of spin-singlet, opposite-spin triplet and equal-spin triplets, respectively. In this work, we are interested in the induced local pairing amplitudes $\tilde{f}_s^+(z) \equiv \tilde{f}_s^+(z, z' = z)$ at the interfaces and in the WSM regions. The local pairing amplitudes in the left WSM region ($z = z' \leq z_L$) can be found explicitly as

$$\tilde{f}_0^+(z) = \frac{i a_1}{4 J_e k_e} [(J_e J_h + k_\parallel^2 e^{2i\theta_k}) \sin \alpha - (J_e - J_h) k_\parallel e^{i\theta_k} \cos \alpha] e^{-i(k_e + k_h)z}, \quad (22a)$$

$$\tilde{f}_z^+(z) = -\frac{i a_1}{4 J_e k_e} [(J_e J_h - k_\parallel^2 e^{2i\theta_k}) \sin \alpha - (J_e + J_h) k_\parallel e^{i\theta_k} \cos \alpha] e^{-i(k_e + k_h)z}, \quad (22b)$$

$$\tilde{f}_{\uparrow\uparrow}^+(z) = -\frac{i J_h a_1}{2 J_e k_e} (J_e \cos \alpha - k_\parallel e^{i\theta_k} \sin \alpha) \times e^{-i(k_e + k_h)z}, \quad (22c)$$

$$\tilde{f}_{\downarrow\downarrow}^+(z) = -\frac{i k_\parallel e^{i\theta_k} a_1}{2 J_e k_e} (J_e \sin \alpha + k_\parallel e^{i\theta_k} \cos \alpha) \times e^{-i(k_e + k_h)z}. \quad (22d)$$

The ones in the right WSM region ($z = z' \geq z_R$) are related to the Andreev reflection amplitude a_3 . Using $a_3(\alpha, \theta_k) = a_1(-\alpha, -\theta_k)$, they can be obtained from Eqs. (22a-22d) by the relations

$$\tilde{f}_{0/z}^+(z)|_{\mathbf{k}_\parallel, \alpha} = \mp \tilde{f}_{0/z}^+(-z)|_{-\mathbf{k}_\parallel, -\alpha}, \quad (23a)$$

$$\tilde{f}_{\uparrow\uparrow/\downarrow\downarrow}^+(z)|_{\mathbf{k}_\parallel, \alpha} = \tilde{f}_{\downarrow\downarrow/\uparrow\uparrow}^+(-z)|_{-\mathbf{k}_\parallel, -\alpha}. \quad (23b)$$

The local pairing amplitudes stem from Andreev reflection at the interfaces, as indicated by their proportionality to the Andreev reflection amplitudes a_1 or a_3 .

To analyze the weights of different pairing components, we define the averaged amplitudes as

$$f_s^+(z) \equiv \left| \sum_{\mathbf{k}_\parallel} \tilde{f}_s^+(z) |_{\mathbf{k}_\parallel, \alpha} \right|, \quad s \in \{0, z, \uparrow\uparrow, \downarrow\downarrow\}, \quad (24)$$

where the sum runs over all available modes that allow for local or crossed Andreev reflection to happen, i.e., the processes in which Cooper pairs are created. These quantities measure the amount of induced Cooper pairs of spin singlet, opposite-spin triplet and two equal-spin triplets, respectively.

Before considering the influence of the CCP, it is also instructive to discuss some important features in the absence of a CCP. The pairing amplitudes at the left interface $z = z_L$ for the block \mathcal{H}^+ are plotted in Fig. 5 as functions of the angle α and energy ε . First, all the averaged amplitudes are even functions of ε . With increasing $|\varepsilon|$, $f_{0/z}^+(z_L)$ decay monotonically to zero since the superconducting effect decreases away from the Fermi energy. Second, the module of the two opposite-spin amplitudes, namely, the spin-singlet $f_0^+(z_L)$ and opposite-spin triplet $f_z^+(z_L)$, are identical. This results from the fact that for the block \mathcal{H}^+ , the only available reflected hole states moving away from the left interface are polarized with spin up. Third, both $f_{0/z}^+(z_L)$ vanish at $\alpha = 0, \pi$ whereas maximize at $\alpha = \pi/2$ and $3\pi/2$, and they are π -periodic in α , as shown in Fig. 5(a). This feature, similar to the conductances, stems from the α -dependent effective superconducting gap. In addition, we find that the opposite-spin amplitudes at the right interface are equal to the ones at the left interface, $f_{0/z}^+(z_L) = f_{0/z}^+(z_R)$, due to a symmetry of \mathcal{H}^+ indicated by

$$\sigma_z \mathcal{H}^+(\mathbf{k}_\parallel, k_z, \alpha) \sigma_z = -\mathcal{H}^+(\mathbf{k}_\parallel, -k_z, -\alpha). \quad (25)$$

Notably, the same behavior occurs for the other block \mathcal{H}^- .

More intriguing features can be found with respect to the equal-spin amplitudes $f_{\uparrow\uparrow}^+$ and $f_{\downarrow\downarrow}^+$. First of all, both $f_{\uparrow\uparrow/\downarrow\downarrow}^+(z_L)$ vanish not only near $\alpha = 0, \pi$ but also at $\alpha = \pi/2, 3\pi/2$, as shown in Fig. 5(b) and (c). The vanishing at $\alpha = 0, \pi$ is because of the effective pairing potential being zero in the superconductor and no superconductivity being present for any \mathbf{k}_\parallel , whereas the vanishing at $\alpha = \pi/2, 3\pi/2$ is due to a restoration of a C_4 symmetry with respect to \hat{z} direction such that the equal-spin amplitudes from all \mathbf{k}_\parallel average to zero. With increasing energy ε , both $f_{\uparrow\uparrow/\downarrow\downarrow}^+(z_L)$ decay to zero, similar to the opposite-spin amplitudes. However, they are no longer monotonic functions of ε . More interestingly, $f_{\uparrow\uparrow}^+$ is quite different from $f_{\downarrow\downarrow}^+$ at the same interface, due to the splitting of spin degeneracy by the strong spin-orbit coupling in the system. While $f_{\downarrow\downarrow}^+(z_L)$ is at least one order in magnitude smaller than the opposite-spin

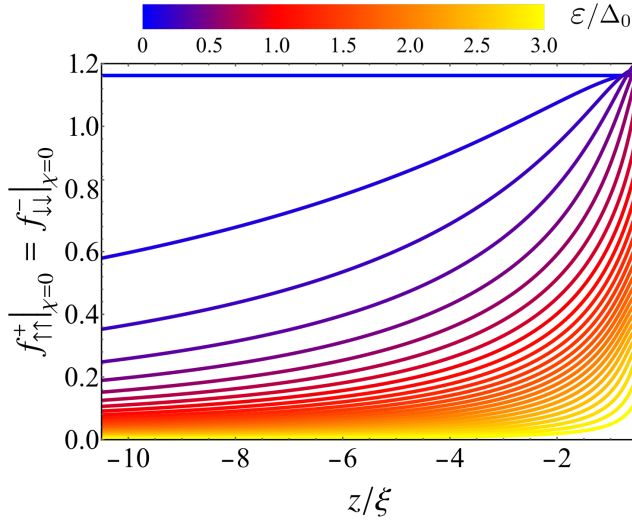


Fig. 6. Position dependence of the equal-spin pairing amplitudes $f_{\uparrow\uparrow}^+$ and $f_{\downarrow\downarrow}^-$ in the left WSM region for various energies ϵ and vanishing χ . For all except the zero energy, the amplitudes decay exponentially to zero in the WSM region. Here, $\alpha = \pi/4$ and other parameters are the same as those in Fig. 5.

amplitudes $f_{0/z}^+(z_L)$, $f_{\uparrow\uparrow}^+(z_L)$ is of the same order, see Fig. 5(b) and (c). Therefore, we have a local spin polarization of Cooper pairs from \mathcal{H}^+ . Again in contrast to $f_{0/z}^+(z_L)$, $f_{\uparrow\uparrow}^+(z_L)$ at the left interface is different from $f_{\uparrow\uparrow}^+(z_R)$ at the right interface. It is, however, equal to $f_{\downarrow\downarrow}^-(z_R)$ at the right interface, and vice versa. Explicitly,

$$f_{\uparrow\uparrow/\downarrow\downarrow}^+(z_L) = f_{\downarrow\downarrow/\uparrow\uparrow}^-(z_R), \quad (26)$$

which can also be related to the symmetry in Eq. (25) that flips the spins.

We next consider the equal-spin amplitudes away from the interfaces in the WSM regions. The equal-spin amplitudes $f_{\uparrow\uparrow}^+(z)$ and $f_{\downarrow\downarrow}^-(z)$ as functions of position z inside the left WSM region for various ϵ are presented in Fig. 6. Here, we choose $\alpha = \pi/4$ in order to optimize the equal-spin amplitudes. In general, $f_{\uparrow\uparrow}^+(z)$ and $f_{\downarrow\downarrow}^-(z)$ decay monotonically away from the interface into the WSM region. However, it is interesting to find that at zero energy, $f_{\uparrow\uparrow}^+(z)$ and $f_{\downarrow\downarrow}^-(z)$ remain almost the same values as the ones at the interface, even deep inside the WSM regions. This can be understood from the position dependence in the amplitudes. Take \mathcal{H}^+ for illustration. The position dependence is contained in a phase factor

$$f_{\uparrow\uparrow}^+(z) \propto e^{-i(k_e+k_h)z}, \quad (27)$$

according to Eqs. (22). At zero energy, the electron and hole wave vectors become exactly opposite, $k_h = -k_e$, for any \mathbf{k}_{\parallel} . Then, the phase factor simply evaluates to unity and the position dependence disappears. Therefore, for small energies we expect considerable equal-spin pairings and a spin polarization of Cooper pairs from the block

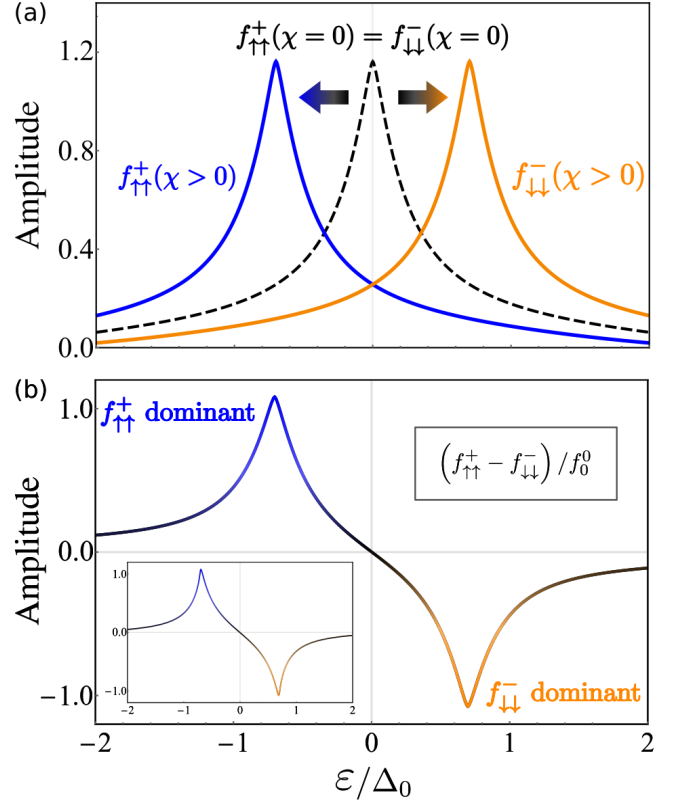


Fig. 7. (a) Equal-spin pairing amplitudes $f_{\uparrow\uparrow}^+$ and $f_{\downarrow\downarrow}^-$ in the left WSM region at $z = -5\xi$ for vanishing (black and dashed line) and a finite (blue and orange lines) CCP $\chi = 0.7\Delta_0$. (b) The finite CCP results in a large net spin polarization of Cooper pairs at $\epsilon \approx \pm\chi$. Inset: If the CCP is present only in the leads, while absent in the superconductor, then the peak and dip are slightly skewed. Here, $\alpha = \pi/4$ and other parameters are the same as those in Fig. 5.

\mathcal{H}^+ inside the WSM regions. For the other block \mathcal{H}^- , we find, however, that the situation is exactly opposite, i.e., $f_{\uparrow\uparrow}^-(z) = f_{\downarrow\downarrow}^+(z)$ and $f_{\downarrow\downarrow}^-(z) = f_{\uparrow\uparrow}^+(z)$. Therefore, in total, no net spin polarization of Cooper pairs remains in the entire system.

This scenario is dramatically changed under the influence of a finite CCP. In Fig. 7, we plot the energy dependence of $f_{\uparrow\uparrow}^+(z)$ and $f_{\downarrow\downarrow}^-(z)$ at $z = -5\xi$ for illustration. In the absence of a CCP, $f_{\uparrow\uparrow}^+$ and $f_{\downarrow\downarrow}^-$ are exactly the same and show a pronounced peak at zero energy. In contrast, a CCP χ shifts the excitation spectra of \mathcal{H}^{\pm} oppositely. As a result, $f_{\uparrow\uparrow}^+$ and $f_{\downarrow\downarrow}^-$ are no longer degenerate but shifted oppositely by $\mp\chi$ in ϵ , as shown in Fig. 7(a). The perfect cancellation of the spin polarizations of Cooper pairs from the two blocks \mathcal{H}^{\pm} is violated. The peak of $f_{\uparrow\uparrow}^+$ is moved to $\epsilon = -\chi$, whereas the peak of $f_{\downarrow\downarrow}^-$ is moved oppositely to $\epsilon = \chi$. In the zero and large energy limits, $f_{\uparrow\uparrow}^+(z)$ and $f_{\downarrow\downarrow}^-(z)$ still coincide and thus no spin polarization exists. However, at energies around $\pm\chi$, $f_{\uparrow\uparrow}^+(z)$ and $f_{\downarrow\downarrow}^-(z)$ are crucially different, leading to a large net spin polarization of Cooper pairs which is given

by the difference of the two total equal-spin amplitudes $f_{\uparrow\uparrow}(z) = f_{\uparrow\uparrow}^+(z) + f_{\uparrow\uparrow}^-(z)$ and $f_{\downarrow\downarrow}(z) = f_{\downarrow\downarrow}^+(z) + f_{\downarrow\downarrow}^-(z)$. Note that $f_{\downarrow\downarrow}^+(z)$ and $f_{\uparrow\uparrow}^-(z)$ remain negligibly small in the left WSM region. Figure 7(b) illustrates the spin polarization $f_{\uparrow\uparrow}(z) - f_{\downarrow\downarrow}(z)$ of Cooper pairs in \hat{z} direction for a positive χ . The spin polarization is negative for positive energies whereas it is positive for negative energies. Importantly, it exhibits a sharp peak and a dip at $\varepsilon = \mp\chi$ as $f_{\uparrow\uparrow}^+(z)$ and $f_{\downarrow\downarrow}^-(z)$ dominate the equal-spin pairings, respectively, which indicates the large spin polarization of Cooper pairs. Since at $\varepsilon = \mp\chi$, the values $f_{\uparrow\uparrow}^+(z)$ and $f_{\downarrow\downarrow}^-(z)$ remain almost the same when the position z is moved more inside the WSM region, the large spin polarization persists deep inside the WSM region. In the other WSM region, we find a similar but opposite net spin polarization of Cooper pairs as the CCP preserves the symmetry in Eq. (25). Therefore, the hybrid junction realizes a dipole of spin-polarized Cooper pairs.

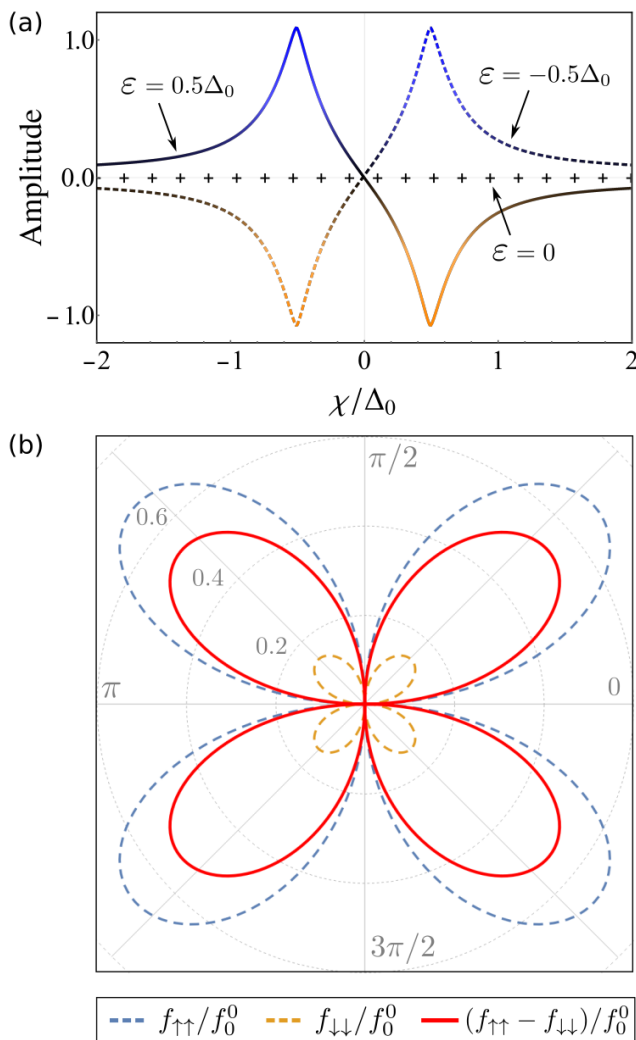


Fig. 8. Spin polarization $f_{\uparrow\uparrow} - f_{\downarrow\downarrow}$ at $z = -5\xi$ as a function of (a) the CCP χ for different choices of energy ε with $\alpha = \pi/4$ and (b) the angle α with $\varepsilon = -0.5\Delta_0$ and $\chi = 0.7\Delta_0$. The other parameters are the same as those in Fig. 5.

Finally, we study the dependence of the net spin polarization of Cooper pairs on the two relevant parameters in this work, the strength of the CCP χ and the angle α . Choosing the CCP to be equal everywhere in the junction, χ globally shifts the energies $\varepsilon \rightarrow \varepsilon \pm \chi$ of \mathcal{H}^\pm , respectively. So far, we have fixed χ and varied ω in our analysis. The behaviour of the net spin polarization should, however, not change if ε is fixed and χ is varied instead. This is exactly what we find in Fig. 8(a): choosing, e.g., $\varepsilon = 0.5\Delta_0$, we find the same peaks as in Fig. 7(b), i.e., $f_{\uparrow\uparrow}^+(z)$ dominates at $\chi = -\varepsilon$, while it is $f_{\downarrow\downarrow}^-(z)$ at $\chi = \varepsilon$. Moreover, the zero-energy mode $\varepsilon = 0$ cancels the net spin polarization for all choices of χ as it is the case for a vanishing CCP. This has an interesting experimental consequence, i.e., it does not matter which quantity is fixed and which one is varied, the signature of the net spin polarization is the same. The angle dependence inherits mainly from those in the equal-spin amplitudes in Fig. 5(b) and (c). The spin polarization vanishes for angles α that are integer multiples of $\pi/2$. When α deviates from these values, the spin polarization increases quickly and reaches the maximal value at around $\alpha_m \in \{\pi/4, 3\pi/4, 5\pi/4, 7\pi/4\}$, see Fig. 8(b). The tuning of angle does, however, not result in a qualitative change but alters merely the magnitude in the signature. These dependencies indicate different ways to manipulate the spin polarization of Cooper pairs.

VI. CONCLUSION AND DISCUSSION

To conclude, we have shown that the transport properties and pairing amplitudes in Weyl NSN junctions depend on the angle between the junction direction and the axis separating Weyl nodes. We have also found that a CCP between Weyl nodes of opposite chirality not only modifies the bias dependence of differential conductances, but also produces a spin polarization of Cooper pairs in the WSM regions. The spin polarization is opposite in the two WSM regions and can be controlled by the energy, CCP and angle dependence.

The CCP, which can be introduced either by the chiral anomaly^{8,48,49} or by strain deformation^{50,51}, is a non-equilibrium effect. Nevertheless, we restrict ourselves in this work to a clean system where the relaxation rate due to the inter-node scattering is much smaller than the energy of the applied fields. In this case, we can expect that the CCP persists for a long time and thereafter our results are applicable.

Although the calculation presented here is based on the more realistic assumption of a large chemical potential in the WSM compared to the pairing potential and CCP, we note that the results of the spin polarization of Cooper pairs and its dipolar characteristic are general and not restricted to these assumptions. Moreover, we have also calculated the case in which the CCP is absent in the superconductor, e.g., due to the Meissner effect, and found that our results stay qualitatively the same,

see the inset of Fig. 7(b).

Recently, the time-reversal symmetry broken WSM phase has been proposed theoretically^{6,14,22–25} and confirmed experimentally^{63–65} in many realistic systems. Among these candidates, the magnetic Heusler alloys²² and tetragonal-structured compounds²³, which host only a single pair of largely separated Weyl nodes, may provide promising platforms to detect our predictions.

VII. ACKNOWLEDGMENTS

We thank P. Bureset, F. Dominguez, and F. Keidel for valuable discussions. This work was supported

by the DFG (SPP1666 and SFB1170 "ToCoTronics"), the Würzburg-Dresden Cluster of Excellence ct.qmat, EXC2147, project-id 39085490, and the Elitenetzwerk Bayern Graduate School on "Topological Insulators".

-
- * song-bo.zhang@physik.uni-wuerzburg.de
- ¹ P. Hosur and X. Qi, *C. R. Phys.* **14**, 857 (2013).
 - ² A. M. Turner and A. Vishwanath, [arXiv:1301.0330](https://arxiv.org/abs/1301.0330).
 - ³ B. A. Bernevig, *Nat. Phys.* **11**, 698 (2015).
 - ⁴ A. A. Burkov, *Nat. Mater.* **15**, 1145 (2016).
 - ⁵ N. P. Armitage, E. J. Mele, and A. Vishwanath, *Rev. Mod. Phys.* **90**, 015001 (2018).
 - ⁶ X. Wan, A. M. Turner, A. Vishwanath, and S. Y. Savrasov, *Phys. Rev. B* **83**, 205101 (2011).
 - ⁷ S. A. Parameswaran, T. Grover, D. A. Abanin, D. A. Pesin, and A. Vishwanath, *Phys. Rev. X* **4**, 031035 (2014).
 - ⁸ H. B. Nielsen and M. Ninomiya, *Phys. Lett. B* **130**, 389 (1983).
 - ⁹ A. A. Zyuzin and A. A. Burkov, *Phys. Rev. B* **86**, 115133 (2012).
 - ¹⁰ D. T. Son and B. Z. Spivak, *Phys. Rev. B* **88**, 104412 (2013).
 - ¹¹ A. A. Burkov, *Phys. Rev. Lett.* **113**, 247203 (2014).
 - ¹² H.-Z. Lu, S.-B. Zhang, and S.-Q. Shen, *Phys. Rev. B* **92**, 045203 (2015).
 - ¹³ S.-B. Zhang, H.-Z. Lu, and S.-Q. Shen, *New J. Phys.* **18**, 053039 (2016).
 - ¹⁴ A. A. Burkov and L. Balents, *Phys. Rev. Lett.* **107**, 127205 (2011).
 - ¹⁵ G. B. Halász and L. Balents, *Phys. Rev. B* **85**, 035103 (2012).
 - ¹⁶ M. Hirayama, R. Okugawa, S. Ishibashi, S. Murakami, and T. Miyake, *Phys. Rev. Lett.* **114**, 206401 (2015).
 - ¹⁷ H. M. Weng, C. Fang, Z. Fang, B. A. Bernevig, and X. Dai, *Phys. Rev. X* **5**, 011029 (2015).
 - ¹⁸ S. M. Huang, S. Y. Xu, I. Belopolski, C. C. Lee, G. Chang, B. K. Wang, N. Alidoust, G. Bian, M. Neupane, C. Zhang, S. Jia, A. Bansil, H. Lin, and M. Z. Hasan, *Nat. Commun.* **6**, 7373 (2015).
 - ¹⁹ T. Rauch, S. Achilles, J. Henk, and I. Mertig, *Phys. Rev. Lett.* **114**, 236805 (2015).
 - ²⁰ J. Ruan, S.-K. Jian, H. Yao, H. Zhang, S.-C. Zhang, and D. Xing, *Nat. Commun.* **7**, 11136 (2016).
 - ²¹ J. Ruan, S.-K. Jian, D. Zhang, H. Yao, H. Zhang, S.-C. Zhang, and D. Xing, *Phys. Rev. Lett.* **116**, 226801 (2016).
 - ²² Z. Wang, M. G. Vergniory, S. Kushwaha, M. Hirschberger, E. V. Chulkov, A. Ernst, N. P. Ong, R. J. Cava, and B. A. Bernevig, *Phys. Rev. Lett.* **117**, 236401 (2016).
 - ²³ Y. J. Jin, R. Wang, Z. J. Chen, J. Z. Zhao, Y. J. Zhao, and H. Xu, *Phys. Rev. B* **96**, 201102(R) (2017).
 - ²⁴ H. Yang, Y. Sun, Y. Zhang, W.-J. Shi, S. S. P. Parkin, and B. Yan, *New J. Phys.* **19**, 015008 (2017).
 - ²⁵ G. Chang, B. Singh, S.-Y. Xu, G. Bian, S.-M. Huang, C.-H. Hsu, I. Belopolski, N. Alidoust, D. S. Sanchez, H. Zheng, H. Lu, X. Zhang, Y. Bian, T.-R. Chang, H.-T. Jeng, A. Bansil, H. Hsu, S. Jia, T. Neupert, H. Lin, and M. Z. Hasan, *Phys. Rev. B* **97**, 041104(R) (2018).
 - ²⁶ S. Y. Xu, I. Belopolski, N. Alidoust, M. Neupane, G. Bian, C. L. Zhang, R. Sankar, G. Q. Chang, Z. J. Yuan, C. C. Lee, S. M. Huang, H. Zheng, J. Ma, D. S. Sanchez, B. K. Wang, A. Bansil, F. C. Chou, P. P. Shibayev, H. Lin, S. Jia, and M. Z. Hasan, *Science* **349**, 613 (2015).
 - ²⁷ L. X. Yang, Z. K. Liu, Y. Sun, H. Peng, H. F. Yang, T. Zhang, B. Zhou, Y. Zhang, Y. F. Guo, M. Rahn, D. Prabhakaran, Z. Hussain, S.-K. Mo, C. Felser, B. Yan, and Y. L. Chen, *Nat. Phys.* **11**, 728 (2015).
 - ²⁸ B. Q. Lv, H. M. Weng, B. B. Fu, X. P. Wang, H. Miao, J. Ma, P. Richard, X. C. Huang, L. X. Zhao, G. F. Chen, Z. Fang, X. Dai, T. Qian, and H. Ding, *Phys. Rev. X* **5**, 031013 (2015).
 - ²⁹ B. Q. Lv, N. Xu, H. M. Weng, J. Z. Ma, P. Richard, X. C. Huang, L. X. Zhao, G. F. Chen, C. E. Matt, F. Bisti, V. N. Strocov, J. Mesot, Z. Fang, X. Dai, T. Qian, M. Shi, and H. Ding, *Nat. Phys.* **11**, 724 (2015).
 - ³⁰ S. Y. Xu, N. Alidoust, I. Belopolski, Z. Yuan, G. Bian, T. R. Chang, H. Zheng, V. N. Strocov, D. S. Sanchez, G. Chang, C. Zhang, D. Mou, Y. Wu, L. Huang, C. C. Lee, S. M. Huang, B. Wang, A. Bansil, H. T. Jeng, T. Neupert, A. Kaminski, H. Lin, S. Jia, and M. Zahid Hasan, *Nat. Phys.* **11**, 294 (2015).
 - ³¹ N. Xu, H. M. Weng, B. Q. Lv, C. E. Matt, J. Park, F. Bisti, V. N. Strocov, D. Gawryluk, E. Pomjakushina, K. Conder, N. C. Plumb, M. Radovic, G. Autes, O. V. Yazyev, Z. Fang, X. Dai, T. Qian, J. Mesot, H. Ding, and M. Shi, *Nat. Commun.* **7** (2016).
 - ³² L. Fu and C. L. Kane, *Phys. Rev. Lett.* **100**, 096407 (2008).
 - ³³ P. Bureset, B. Lu, G. Tkachov, Y. Tanaka, E. M. Hankiewicz, and B. Trauzettel, *Phys. Rev. B* **92**, 205424 (2015).
 - ³⁴ M. Sato and Y. Ando, *Rep. Prog. Phys.* **80**, 076501 (2017).
 - ³⁵ C. Fleckenstein, N. T. Ziani, and B. Trauzettel, *Phys. Rev. B* **97**, 134523 (2018).

- ³⁶ J. Linder and J. W. Robinson, *Nat. Phys.* **11**, 307 (2015).
- ³⁷ D. Breunig, P. Buset, and B. Trauzettel, *Phys. Rev. Lett.* **120**, 037701 (2018).
- ³⁸ W. Chen, L. Jiang, R. Shen, L. Sheng, B. G. Wang, and D. Y. Xing, *Europhys. Lett.* **103**, 27006 (2013).
- ³⁹ S. Uchida, T. Habe, and Y. Asano, *J. Phys. Soc. Jpn.* **83**, 064711 (2014).
- ⁴⁰ U. Khanna, A. Kundu, S. Pradhan, and S. Rao, *Phys. Rev. B* **90**, 195430 (2014).
- ⁴¹ N. Bovenzi, M. Breitzkreiz, P. Baireuther, T. E. O'Brien, J. Tworzydło, I. Adagideli, and C. W. J. Beenakker, *Phys. Rev. B* **96**, 035437 (2017).
- ⁴² A. Chen, D. I. Pikulin, and M. Franz, *Phys. Rev. B* **95**, 174505 (2017).
- ⁴³ S.-B. Zhang, F. Dolcini, D. Breunig, and B. Trauzettel, *Phys. Rev. B* **97**, 041116(R) (2018).
- ⁴⁴ K. A. Madsen, E. J. Bergholtz, and P. W. Brouwer, *Phys. Rev. B* **95**, 064511 (2017).
- ⁴⁵ S.-B. Zhang, J. Erdmenger, and B. Trauzettel, *Phys. Rev. Lett.* **121**, 226604 (2018).
- ⁴⁶ M. Alidoust, *Phys. Rev. B* **98**, 245418 (2018).
- ⁴⁷ S. Uddin, W. Duan, J. Wang, Z. Ma, and J.-F. Liu, *Phys. Rev. B* **99**, 045426 (2019).
- ⁴⁸ K. Fukushima, D. E. Kharzeev, and H. J. Warringa, *Phys. Rev. D* **78**, 074033 (2008).
- ⁴⁹ Q. Li, D. E. Kharzeev, C. Zhang, Y. Huang, I. Pletikoscic, A. V. Fedorov, R. D. Zhong, J. A. Schneeloch, G. D. Gu, and T. Valla, *Nat. Phys.* **12**, 550 (2016).
- ⁵⁰ Z. Song, J. Zhao, Z. Fang, and X. Dai, *Phys. Rev. B* **94**, 214306 (2016).
- ⁵¹ A. Cortijo, D. Kharzeev, K. Landsteiner, and M. A. H. Vozmediano, *Phys. Rev. B* **94**, 241405(R) (2016).
- ⁵² A. A. Zyuzin, S. Wu, and A. A. Burkov, *Phys. Rev. B* **85**, 165110 (2012).
- ⁵³ W. L. McMillan, *Phys. Rev.* **175**, 559 (1968).
- ⁵⁴ G. E. Blonder, M. Tinkham, and T. M. Klapwijk, *Phys. Rev. B* **25**, 4515 (1982).
- ⁵⁵ S. Kashiwaya and Y. Tanaka, *Rep. Prog. Phys.* **63**, 1641 (2000).
- ⁵⁶ T. Meng and L. Balents, *Phys. Rev. B* **86**, 054504 (2012).
- ⁵⁷ S. A. Yang, H. Pan, and F. Zhang, *Phys. Rev. Lett.* **113**, 046401 (2014).
- ⁵⁸ C. W. J. Beenakker, *Three "Universal" Mesoscopic Josephson Effects* (Springer, Berlin, 1992) pp. 235–253.
- ⁵⁹ J. Cayssol, *Phys. Rev. Lett.* **100**, 147001 (2008).
- ⁶⁰ C. J. Lambert, V. C. Hui, and S. J. Robinson, *J. Phys. Cond. Matter* **5**, 4187 (1993).
- ⁶¹ M. P. Anantram and S. Datta, *Phys. Rev. B* **53**, 16390 (1996).
- ⁶² In this work, we consider the transport in the NSN junction as a two-terminal scattering problem. This is perfectly justified in the sub-gap regime where Cooper pairs govern the transport in the superconductor. In experiments, quasi-particles may escape into the superconducting lead, especially in the supra-gap regime, which may modify the results quantitatively. However, our treatment should be valid if the quasi-particle escape is small compared to other transport processes.
- ⁶³ M. Hirschberger, S. Kushwaha, Z. Wang, Q. Gibson, S. Liang, C. A. Belvin, B. Bernevig, R. Cava, and N. Ong, *Nat. Mater.* **15**, 1161 (2016).
- ⁶⁴ K. Kuroda, T. Tomita, M.-T. Suzuki, C. Bareille, A. Nugroho, P. Goswami, M. Ochi, M. Ikhlas, M. Nakayama, S. Akebi, *et al.*, *Nat. Mater.* **16**, 1090 (2017).
- ⁶⁵ A. Sakai, Y. P. Mizuta, A. A. Nugroho, R. Sihombing, T. Koretsune, M.-T. Suzuki, N. Takemori, R. Ishii, D. Nishio-Hamane, R. Arita, *et al.*, *Nat. Phys.* **14**, 1119 (2018).